ISSN 2176-5480

22nd International Congress of Mechanical Engineering (COBEM 2013)
November 3-7, 2013, Ribeirão Preto, SP, Brazil

DESIGN OF A SHUNTED ISOLATOR FOR REDUCTION OF THE VIBRATION TRANSMISSION OF A PLANE FUSELAGE

Torsten Bartel
Oliver Heuss
Dirk Mayer
Tobias Melz
Fraunhofer LBF, Darmstadt, Germany
torsten.bartel@lbf.fraunhofer.de

Francisco Scinocca
Airton Nabarrete
Luiz Carlos Sandoval Goes
Instituto Tecnológico de Aeronáutica, São José dos Campos, SP, Brasil

Abstract. *This paper presents the design process and measurement results of a shunted piezoelectric isolator, which can be a good compromise between an solely passive and an active isolator. The system will be used for the reduction of the vibration transmission between two idealized panels of a plane fuselage. By an experimental modal analysis of the panel,the modal behavior is investigated. The modal data is used to derrive a state-space description of the panel, which is included into a system simulation environment. Consequently, the shunted piezoelectric isolator is principally designed. By an analytical description, the isolator beam is automatically optimized to defined goal parameters. Applying an impedance-admittance simulation approach, both the isolator and the shunt can be modelled. Using the simulation environment, the configuration and the performance of the shunt can be investigated and adjusted. After hardware realization of the shunted isolator, it is examined in a test setup. Obtained masurement results are compared to simulation results of the system. The paper shows the usefulness of a shunted piezoelectric element in addition to a passive isolation system. Furthermore an effective preliminary design strategy for the layout of shunted piezoelectric isolators is presented.*

Keywords: *smart material, vibration isolation, shunt damping, semi active system*

1. INTRODUCTION

The design of modern technical systems is highly affected by the increase of performance and by the usage of lightweight methods, while there are higher restrictions and demands on noise and vibration levels. In more and more applications, these contrary requirements cannot be countered by solely passive measures. In this case, systems for active vibration reduction are used under the restriction of the necessity of a power supply (Fuller, et al., 1997). However, by the usage of these systems, a significant improvement of the relationship between weight and power can be achieved, thus gaining an advantage in lightweight structure, such as aircrafts (Konstanzer, et al., 2006), or satellites applications (Bastaits, et al., 2010).

In between the fields of passive and active vibration reduction, there are semi passive systems. Such systems can increase the performance of passive measures without the need for an external power supply (Schmidt, et al., 2011). One approach for a semi passive system is the shunt damping technique associated with piezoelectric materials (Hagood and von Flotow, 1991).

This present paper is focused on the vibration reduction using the shunt damping technique in combination with a vibration isolator for reducing the vibration transmission of a typical aeronautical panel, normally applied in commercial aircrafts. The main objective is the reduction of the transmissibility between the outer panel of the aircraft and its interior.

1.1 Shunted damping

The demand on reducing vibrations of lightweight structures led to the development of several active, semi-active and semi-passive techniques in the last decades. Compared to active vibration control, the two latter ones need less energy since they do not need additional actuators in the classical sense. Shunted damping techniques like the resonant Resistance-Inductance shunt (*RL*-shunt) use dissipative effects of an electric circuits for structural damping (Hagood and von Flotow, 1991). Others like the “synchronised switched damping on inductance” technique (SSDI) invert the piezoelectric charges on the electrodes of the piezoelectric ceramic transducer by coupling a resonant shunt for a short periods of time when the maximum deformation is approximately reached (Corr and Clark, 2001). That way the resulting forces lead to higher damping values of the host structure. There exist plenty of different related techniques briefly summed up below. They all need whether no additional energy or just little energy for the supply of the active electrical components, e.g. operational amplifiers. Since their functional behavior is closely related to the one of the host structure, the performance depends strongly on an appropriate design and also on the given excitation scenario.

ISSN 2176-5480

Compared to passive and active measures, both semi-active and semi-passive solutions are not capable of inducing comparable broadband damping effects. However several approaches, e.g. the Resistance shunt connected to a negative capacity (*RC*-shunt) (Behrens, et al., 2003), patented by (Forward, 1979), raise the damping efficiency over a broad frequency range. Wu and Bicos (1997) additionally connect an inductance, leading to the behavior of an *RL*-shunt with an actively increased generalized electromechanical coupling coefficient which describes the amount of energy that can be transferred from the mechanical to the electrical system side. In a first approximation, the structural behavior of the below described vibration isolator can be described as steady in terms of Eigenfrequencies. Thus, a system with minimal energy consumption can be realized. In the following, this paper focuses on the classical semi-passive *RL*-shunt technique introduced by (Hagood and von Flotow, 1991). Principally, shunt designs can also be extended to an adaptable absorption frequency in order to automatically compensate e.g. thermal changes of the environment (Niederberger, 2005).

The principal of a *RL*-shunted piezoelectric transducer is shown in Fig. 1 a). The transducer is simplified as a capacitance and a voltage source. The shunt consists of a resistor and an inductor.

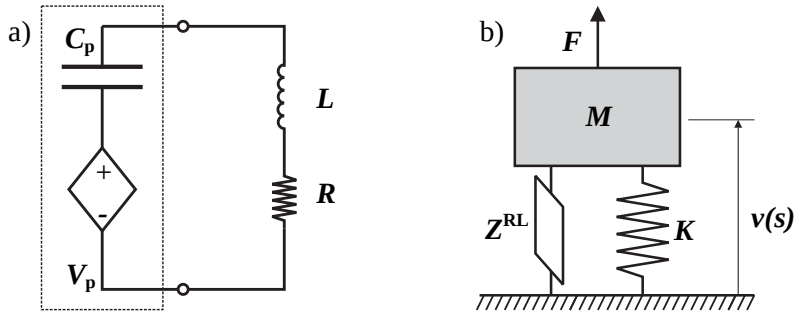

Figure 1. Principle of an RL-shunted system
a) Electrical oscillator circuit consisting of a piezoelectric element and a series RL-shunt
b) Mechanical model of a 1-DOF oscillator with RL-Shunt

When coupled to an undamped one-degree of freedom mass oscillator, as shown in Fig. 1 b), the admittance of the shunted system (Hagood and von Flotow, 1991) is given by Eq. (1) according to

$$\frac{v(s)}{F(s)} = \frac{1}{Ms + (K/s) + Z_{jj}^{RL}(s)}. \tag{1}$$

The relation of the velocity v to Force F is defined by the modal mass M, the modal stiffness K and the impedance contribution Z_{jj}^{RL} of the RL-shunt. The latter is defined through Eq. (2) as

$$Z_{jj}^{RL}(s) = 1 - k_{ij}^2\left(\frac{\delta^2}{\gamma^2 + \delta^2 r\gamma + \delta^2}\right) \tag{2}$$

with
k_{ij} = material electromechanical coupling coefficient
γ = s/ω_0^E = non-dimensional frequency
ω_n^E = mechanical Eigenfrequency of the 1-DOF System with the piezoelectric element open circuited
δ = ω_e/ω_n
ω_e = electrical Eigenfrequency of the RL-shunted piezoelectric element
ω_n = mechanical Eigenfrequency of the 1-DOF System
r = $R_i C_{pi}^S \omega_n^E$ = dissipation tuning parameter
C_{pi}^S = inherent capacitance of the piezoelectric shunted in the *i*th direction at constant strain (clamped).

ISSN 2176-5480

1.2 Active and passive vibration isolation

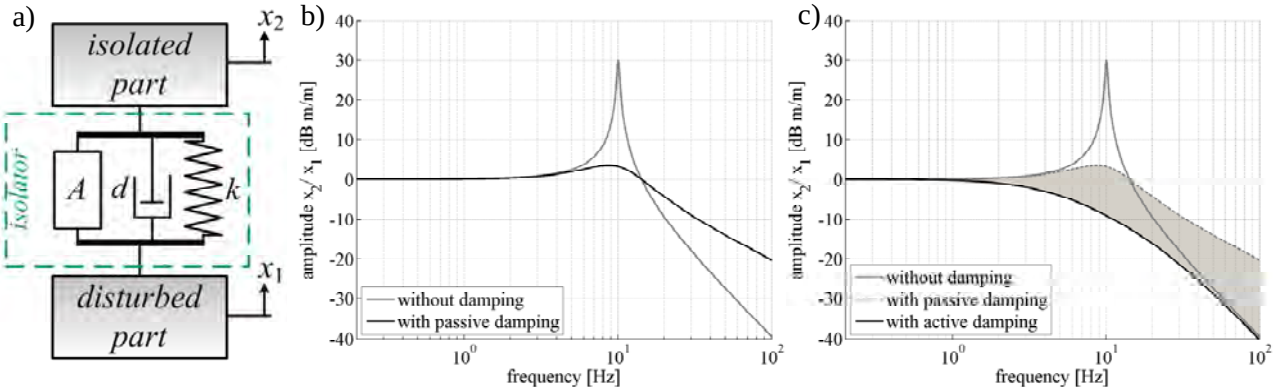

Figure 2. Transmissibility curves of an isolation system for passive and active vibration isolation
a) Scheme of an isolation system
b) Passive isolation
c) Active isolation

For vibration isolation, the mechanical path between a disturbance source and the structure that is to be isolated has to be designed. The design follows such way that a vibration reduction is yielded in a certain frequency range. This can be achieved by adding a stiffness element *k*, a damping element *d* and, if required, an actuator element *A*. The scheme of an isolation system is depicted in Fig. 2 a).

Regarding the transmissibility of a passive isolation system between a disturbed part and an isolated part, the typical amplitude response is given in Fig. 2 b). As shown, the undamped isolator effects an increasing vibration isolation of -40 dB per decade in the frequency range above the resonance of the mass-spring system. An arising drawback is the vibration amplification in the region of the resonance frequency. The amplification can be reduced by the integration of a damper which however also reduces the isolation effect at higher frequencies.

In addition to passive isolation, active isolation unites the advantages of damped and undamped systems as can be seen in Fig. 2 c). While broadband isolation remains at frequencies above the resonance, the amplitude amplification in the resonance can be reduced equal to the effect of a damping element (Preumont, 2011).

1.3 Principle of the shunted vibration isolation

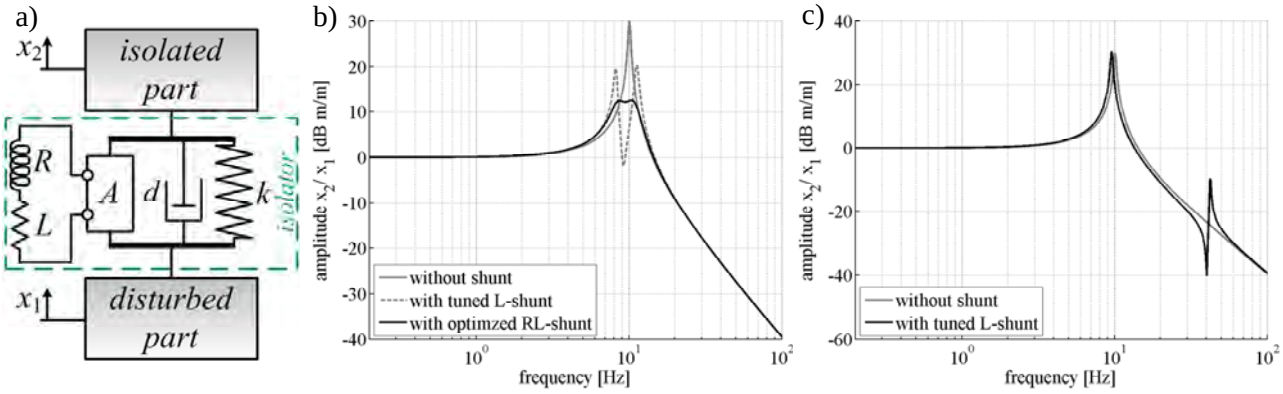

Figure 3. Transmissibility curves of a shunted isolation system
a) Scheme of an shunted isolation system
b) Damped absorption of the resonance amplification
c) Neutralization of a single harmonic excitation

Besides all advantages, the necessity of power amplifiers for the actuators is a negative aspect of active isolation systems, making them unfeasible for certain applications. A compromise between passive and active isolation can be the integration of a shunted electric circuit as described above, i.e. a shunted electromagnetic transducer (de Marneffe, et al., 2008). The scheme of an *RL*-shunted piezoelectric isolator is shown in Fig. 3 a).

ISSN 2176-5480

Two possibilities to adjust an *RL*-shunt base on the absorption of the resonance amplification and on the neutralization of a single harmonic excitation as shown in Fig. 3 b) and Fig. 3 c) respectively. By tuning and optimizing the *RL*-shunt, an effect similar to a damped vibration absorber is achieved. Thus the resonance amplification can be reduced without a loss of isolation at higher frequencies. The tuning of the shunt to a higher frequency enables the neutralization of a single harmonic excitation. Since the shunt causes additional resonance amplification, the neutralization effect is less suitable for broadband excited system.

1.4 Integration of a shunted isolator into a plane fusselage demonstration setup

The integration of a passive spring-damper element into the transmission path is state of the art in order to achieve vibration isolation between two panels of a plane fuselage (Hidalgo, et al., 2011). In this work, these passive elements are exchanged by a shunted piezoelectric bending beam as presented in Fig. 4. The aim is to prove the principle feasibility of a shunted piezoelectric isolator.

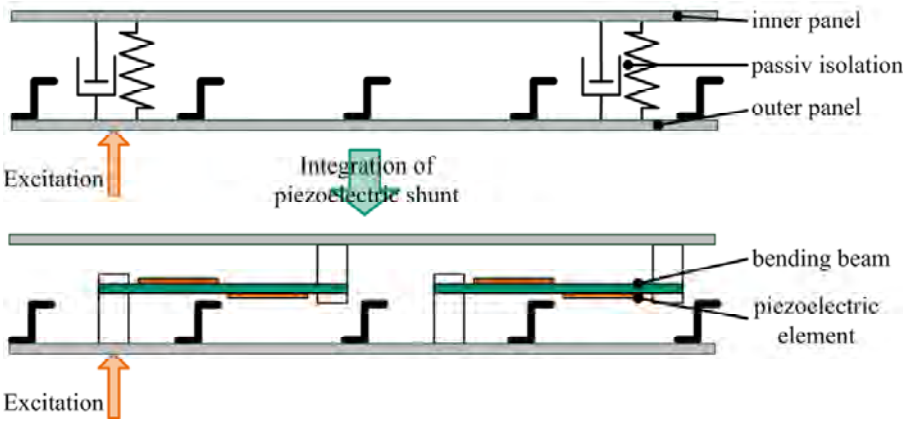

Figure 4. Concept of the integration of a shunted isolator to an airplane fuselage

On base of measured data on an airplane (i.e. Lo, 2002), an idealized but realistic excitation scenario of the outer fuselage structure is assumed. This excitation scenario consists of harmonic and higher order force excitation due to the jet engine and broad banded random force excitation due to the air flow. The harmonic excitation is defined to be 50 Hz (3000 rpm), while the random excitation is broadband from 40 Hz to 160 Hz.

2. CHARACTERIZATION OF THE BASE STRUCTURE

2.1 Setup of the experimental characterization of the aircraft Panel

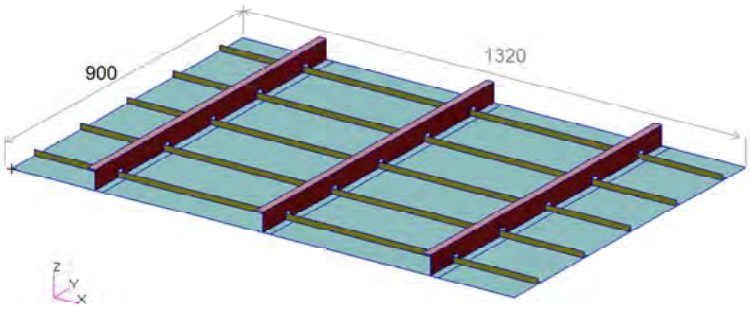

Figure 5. Typical aircraft panel to apply the shunted isolator

According to Fig. 5, an idealized flat panel similar to those, normally applied in the aeronautical industry, is set up in order to conduct the investigation on the effectiveness of the shunted isolator. An experimental modal analysis is performed to analyze the dynamic behavior of the panel structure. For a reasonable definition of the global and local modes in the area between stiffeners, 253 distinct measurement points are chosen. The suspended panel is excited by a shaker, according to Fig. 6 b). Figure 6 a) shows the reflection points that define the measurement grid. In order to measure the dynamic responses curves, a laser vibrometer system is used.

ISSN 2176-5480

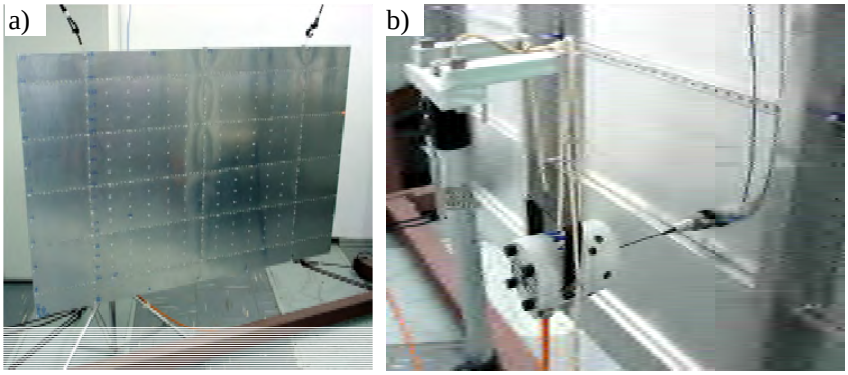

Figure 6. Measurement setup for modal analyses
a) Measurement points at the front side of the aircraft panel
b) Shaker excited backside of the panel

2.2 Experimental modal analysis

The averaged frequency response function and the averaged coherence are shown in Fig. 7.

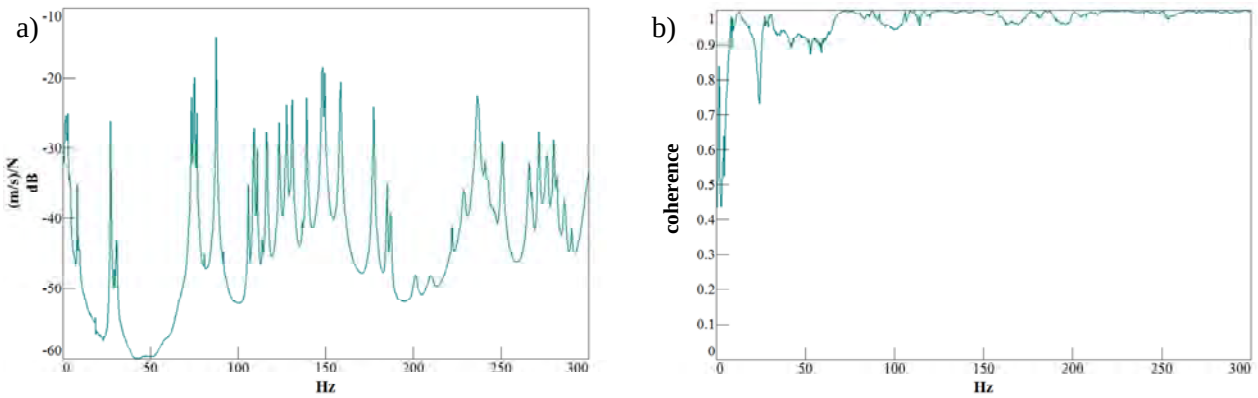

Figure 7. Results of the experimental modal analysis
a) Amplitude of the average frequency response function of 253 points
b) Average coherence of the frequency response functions of 253 points

Above 70 Hz, a relatively high modal density is given. Furthermore the coherence plot gives proof of the reliability of the measurement data to carry out a modal analysis. Using the poly-reference least squares complex frequency domain algorithm (pLSCF), 45 modes and their corresponding modal parameters are identified up to 300 Hz. In the lower frequency range, global modes of the whole panel are dominant. At 8 Hz the first torsional mode is identified.

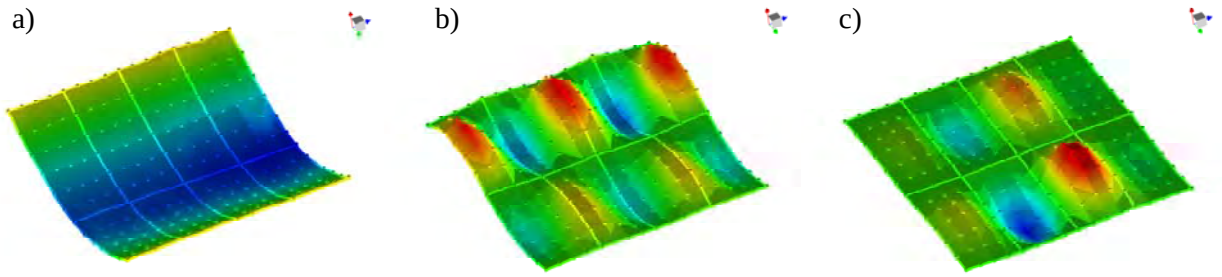

Mode 2 at 27 Hz | Mode 22 at 177 Hz | Mode 21 at 158 Hz

Figure 8. Characteristic mode shapes
a) Global mode shape
b) Stiffener-dominated mode shape
c) Plate-element-dominated mode shape

ISSN 2176-5480

Figure 8 gives an exemplary comparison of characteristic mode shapes. The first bending mode occurs at 27 Hz (Fig. 8 a). In this frequency range the plate behaves similar to a conventional flat panel in free-free condition. In the mode shape shown in Fig. 8 b), the bending of the stiffeners is dominant. Figure 8 c) illustrates a mode shape, in which local deflections of the single plate-elements between the stiffeners are recognizable. The latter type will also appear at higher frequencies at a real fuselage panel.

3. MODELLING AND SIMULATION OF THE SHUNTED SYSTEM

This chapter gives an overview of the used admittance-impedance modeling principle. After the description of the design and the optimization of the shunted isolator, the integration of both the isolator and the base structure into the simulation environment is given.

3.1 Principle of the admittance-impedance formulation of a mechanical system

Following the admittance-impedance approach (Herold, et al., 2006), electrical and the mechanical components are described in an equal manner. While for electrical components this approach is common, the electromechanical analogies are used for the formulation of the mechanical simulation part. Therefore the disturbed and mounted bodies are expressed as admittances, while the juncture elements correspond to impedances as shown in Fig. 9.

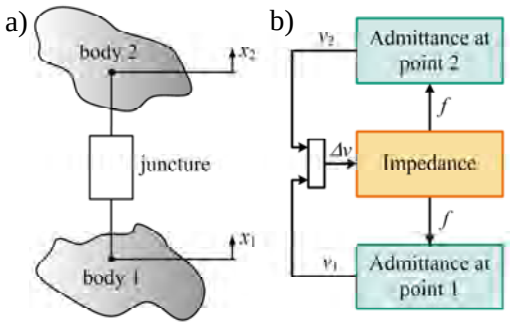

Figure 9. Principle of the mechanical admittance-impedance approach

Internal forces, which are caused by the impedances, and external forces are the input into the admittances. The output is the resulting velocity of the body. The input into the impedances is the difference of the velocities of the adjoined bodies. Their output are the resulting forces.

3.2 Design and optimization of the isolator geometry

In consideration of a low resonance frequency and a high electro-mechanical coupling of the shunted isolation system, a piezoelectric bending beam is a suitable design concept (Bartel, et al., 2012). Figure 10 a) depicts the design scheme of a double sided clamped piezoelectric beam. Due to the bilateral clamping, the deflection curve as shown in Fig. 10 b) results as response to a force at the tip of the beam. The corresponding strain distribution causes the alternating application of the piezoelectric elements.

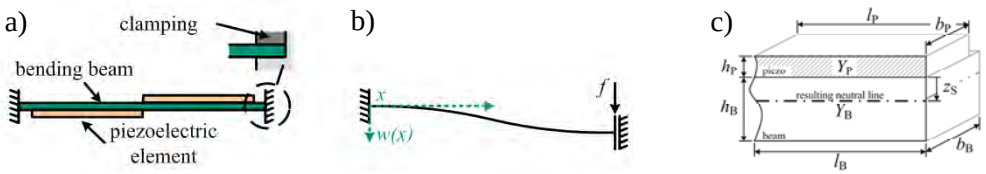

Figure 10. Design concept of the isolator
a) Scheme of the piezoelectric bending beam
b) Deflection curve
c) Geometrical parameters

In order to optimize the geometrical parameters of the piezoelectric bending actuator, as shown in Fig. 10 c), the analytical description according to (Bartel, et al., 2011) is used. Derived from the assumed excitation scenario, the first and second resonance frequencies $f_{e,1}$ and $f_{e,2}$ as well as the voltage to force transduction k_T are chosen as optimization

ISSN 2176-5480

goals. On base of the analytical description, the calculation of the resonance frequencies of the beam follows the solution of the characteristic equation

$$\sinh(\lambda l_B)\cos(\lambda l_B)+\cosh(\lambda l_B)\sin(\lambda l_B)+\sin(\lambda l_B)\cos(\lambda l_B)+\lambda l_B\frac{m}{m_B}\{\cosh(\lambda l_B)\cos(\lambda l_B)-1\}=0 \tag{3}$$

for each numerically evaluable result of the eigenvalue λ according to Hagedorn and DasGupta (2007). The voltage to force transduction k_T is given by

$$k_T=\frac{f_B}{U_P}=\frac{3\cdot Y_P\cdot d_{31}\cdot b_P}{l_B}\cdot\left(z_S+\frac{h_P}{2}\right) \tag{4}$$

and therefore solely depends on material properties, which are the Young's Modulus Y_P and the piezoelectric coupling coefficient d_{31}, and geometrical parameters, which are the length of the beam l_B, the width and height of the piezoelectric element b_P and h_P respectively and the distance of the piezoelectric element to the resulting neutral line z_S. The goal parameter are defined to be

$$\begin{aligned} &f_{e,1}\approx 35\text{ Hz}\\ &f_{e,2}\geq 1.000\text{ Hz}\\ &k_T\mapsto \max. \end{aligned} \tag{5}$$

The optimized parameters are adapted to commercially available raw material of the piezoelectric elements and to the beam thickness. Figure 11 shows the first three solutions of the characteristic equation for the resulting geometry which corresponds to the mode shapes of the beam.

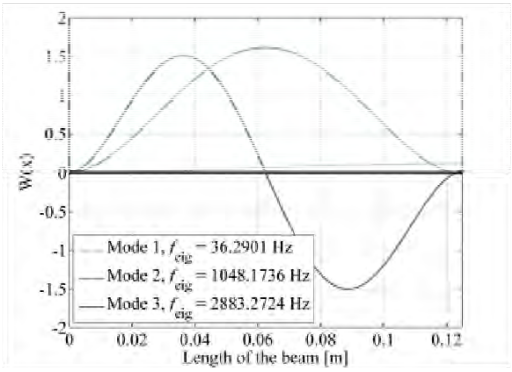

Figure 11. Analytical estimated mode shapes of the optimized piezoelectric bimorph with 1 kg tip mass

As can be seen, the eigenfrequencies are calculated to $f_{e,1}$ = 36,3 Hz and $f_{e,2}$ = 1048 Hz and therefore fit the goal parameters sufficiently. The voltage to force transduction factor is estimated to a maximal value of k_T = 0,19 N/V.

3.3 Simulation of the isolation system

3.3.1 Setup of the simulation model

The simulation model consists of three different parts which are the fuselage panel as excited body, the shunted isolator as juncture element and a secondary plate as isolated body. While the secondary plate is idealized by a ridged body mass, the fuselage panel and the isolator are simulated considering their elastic dynamic behavior.

One approach for the derivation of an admittance model that considers the elastic dynamic behavior of the body bases on the principle of the modal superposition of the influence of single mode shapes (Bartel, et al., 2010) according to

$$\frac{v_l(s)}{f_k(s)}=G_{lk}(s)=\sum_{i=1}^{j}\frac{\phi_{li}\,\phi_{ki}}{s^2+2\nu_i\,\omega_{0i}\,s+\omega_{0i}^2}\,. \tag{6}$$

ISSN 2176-5480

Therein the admittance G_{lk}, which equals the velocity response v(s) at point l to a force f(s) at point k, is calculated by the sum of the admittances of the single modes. Thus, the single admittance of the i[th] mode consists of the Eigenvalue ϕ_{ni} at point n, the modal damping factor ν_i and the Eigenfrequency ω_{0i}.

The modal superposition finally leads to the state-space model

$$\begin{bmatrix} \dot{\vec{x}}(t) \\ \ddot{\vec{x}}(t) \end{bmatrix} = \begin{bmatrix} \underline{0} & \underline{I} \\ diag(\omega_{0i}^2) & diag(2\nu_i\,\omega_{0i}) \end{bmatrix} \cdot \begin{bmatrix} \vec{x}(t) \\ \dot{\vec{x}}(t) \end{bmatrix} + \begin{bmatrix} \underline{\phi}^T \end{bmatrix} \begin{bmatrix} \vec{f}_{\mathrm{Pn}}(t) \end{bmatrix}$$
$$\begin{bmatrix} \vec{v}_{\mathrm{Pn}}(t) \end{bmatrix} = [\underline{0} \quad \underline{\phi}^T] \cdot \begin{bmatrix} \vec{x}(t) \\ \dot{\vec{x}}(t) \end{bmatrix} + [\underline{0}] \begin{bmatrix} \vec{f}_{\mathrm{Pn}}(t) \end{bmatrix} \tag{7}$$

of an elastic body with the input and output points P_n that can be included in the system simulation. The state-space model can be derived only on base of modal data achieved by i.e. measurement or numerical simulation. Together with the above estimated modal data, the given state-space formulation enables the integration of the dynamic behavior of the fuselage panel into the simulation environment. As an example, the admittance at one randomly chosen point of the panel is depicted in Fig. 12.

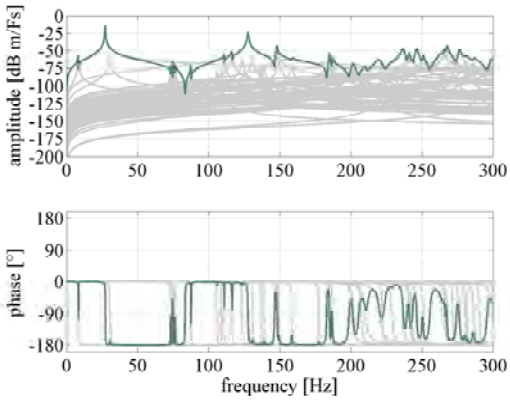

Figure 12. Exemplary point admittance of the excited fuselage panel

The modeling of the isolator can be carried out in a similar way. However, high stiffness elements have to be included additionally, since the isolator has to be modeled as impedance. Furthermore, the electro-mechanical coupling is included by the transfer behavior of the electrical actuator voltage to the equivalent mechanical force. The complete isolator model is schematized in Fig. 13.

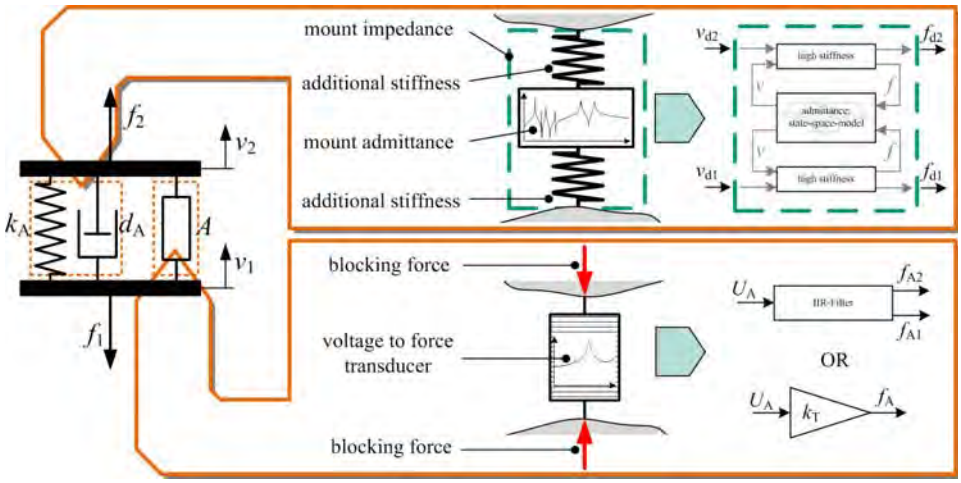

Figure 13. Modeling scheme of the isolator

The purely mechanical part is derived by the state-space model and the modal data. The simulated or measured voltage to force transduction can be estimated by an IIR-Filter or a simple gain factor k_T. While a gain factor is

ISSN 2176-5480

sufficient in the case of an approximately frequency-constant transduction behavior, the IIR-filter enables the simulation of higher dynamic influences.

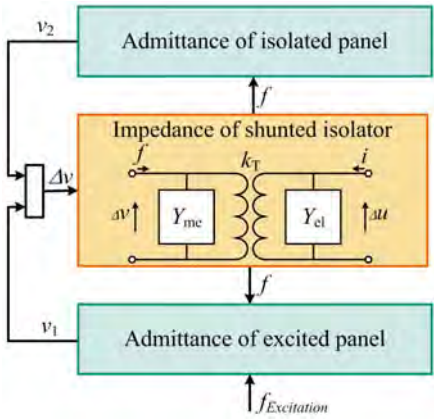

Figure 14. Modeling scheme of a shunted system

Finally the single components are assembled to the shunted system as shown in Fig. 14. The impedance of the shunted isolator combines the impedances of the mechanical system Y_{me} and the electrical system Y_{el}.

3.3.2 Simulation results

Based on the excitation scenario as described in chapter 1.4, one point of the fuselage panel is excited by a force signal according to Fig. 14. As simulation result, the velocity spectra of the excited panel and of the isolated plate are depicted for different shunt configurations in Fig. 15. It can be seen, that in all cases a broad banded isolation that increases to higher frequencies is achieved above approx. 50 Hz.

In Fig. 15 a), the result of the isolation without shunted circuit is shwon. Both the resonance amplification at approx. 35 Hz and the first harmonic at 50 Hz are clearly visible in the velocity spectrum of the plate that is to be isolated. Using an *RL*-shunt that is optimized to 35 Hz, the resonance amplification can be reduced as can be seen in Fig. 15 b). Figure 15 c) illustrates the comparison to an *R*-shunt which is tuned to the harmonic excitation at 50 Hz, thereby resulting in a reduction of the harmonic amplitude. Thus, the simulation results show the principle usage of the shunted isolator for an improved passive isolation of the idealized plane fuselage demonstrator setup.

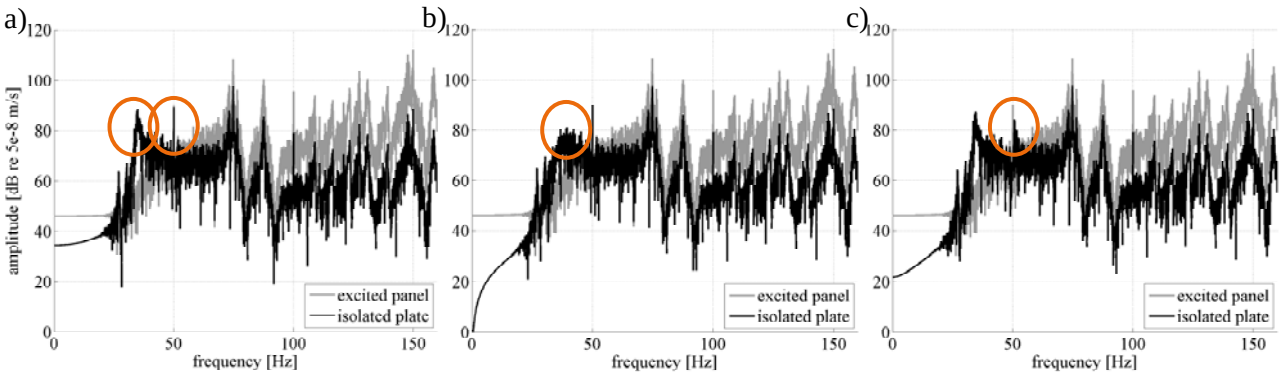

Figure 15. Simulated comparison between the excited panel and the isolated plate
a) Isolation without shunt
b) Isolation with optimized *RL*-shunt in the resonance frequency of the isolator (35 Hz)
c) Isolation with L-shunt, tuned to the first harmonic excitation frequency (50 Hz)

3.4 Layout of the RL-shunt

As described above, the classical *RL*-shunt consists of the piezoelectric element with a capacitive behavior, a passive electrical resistor and an inductance. In order to absorb the first Eigenfrequency at 35 Hz of the vibration isolator, the electrical Eigenfrequency of the shunt has to be tuned to match this frequency. The electrical Eigenfrequency of the shunted system is defined by Eq. (8) according to

ISSN 2176-5480

$$\omega_e = \sqrt{\frac{1}{LC_{pi}^S}} \tag{8}$$

with C_{pi}^S as the inherent capacitance of the clamped piezoelectric element (Hagood and von Flotow, 1991). The combined capacitance of the piezoelectric transducers is 160 nF. With ω_e being 219.9 rad/s, the optimal inductance is calculated by solving Eq. (8) for L, leading to a value of 129.2 H. Such large values cannot be obtained using passive inductors. Therefore a circuit layout proposed by Antoniou (1969) was chosen which synthesizes an inductance by using operational amplifiers and passive electrical parts as resistors and capacitances. The circuit diagram of the synthetic inductor and the finally realized SMD board is shown in Fig. 16. Since the tuning of the shunt to the structural Eigenfrequency is an essential part in order to obtain good damping values, the synthetic inductor L can be adjusted by a potentiometer. This allows values between 0,2 H and 220 H.

Figure 16. Realization of the synthetic inductor
a) Circuit diagram of the inductor (Mayer, et al., 2001)
b) Picture of the SMD circuit board

Furthermore another potentiometer in series to the piezoelectric transducer and the synthetic inductor is integrated to continously change the damping values of the shunted system. The optimal resistance to achive best damping values can be calculated by Eq. (9), given amongst others by Viana and Valder (2006):

$$R = \frac{\sqrt{2}K_{ij}}{C_{pi}^S(1+K_{ij}^2)} \tag{9}$$

K_{ij} descibes the generalized electromechanical coupling coefficient (Hagood and von Flotow, 1991).

4. MEASUREMENT RESULTS OF THE TEST SETUP

Before integrating the shunted isolator into the fuselage demonstrator, a first test setup is implemented to assure both the accuracy of the simulation model and the usability of the hardware realization of the shunted isolator. Therefore, a test setup, showing the shunted isolator and the measurement sensors, is assembled as illustrated in Fig. 17.

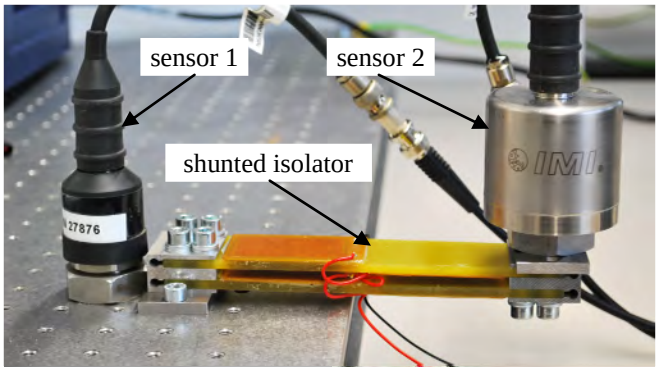

Figure 17. Test setup of the shunted isolator system

ISSN 2176-5480

While the basement (excited part) is excited by a random signal, the transmissibility from the basement to the free oscillating side of the isolator (isolated part) is measured by the shown acceleration sensors. The accelerator at the isolated part serves as sensor as well as system mass, thus causing a resonance frequency at approx. 35 Hz. The simulation model presented in chapter 3.3.1 is simplified to the test setup condition, meaning that a rigid body is considered as exited part.

Figure 18 shows the simulation (Fig. 18 a)) and the measurement results (Fig. 18 b)) of the transmissibility of the isolator according to the test setup and for different shunt configurations. The measurement shows the predicted behavior of the shunted isolator. A tuned *L*-shunt behaves similar to a mechanical vibration absorber, thus causing a new resonance frequency and a zero point at the resonance frequency of the system. Introducing a resistor, the *RL*-shunt adds a damping effect which easily can be tuned to an optimized value. The result is a reduction of the resonance frequency without the loss of isolation at higher frequencies. As comparison shows, the measured behavior can be predicted sufficiently well by the presented simulation model. Therefore the optimization procedure and the simulation model are usable for preliminary design tasks.

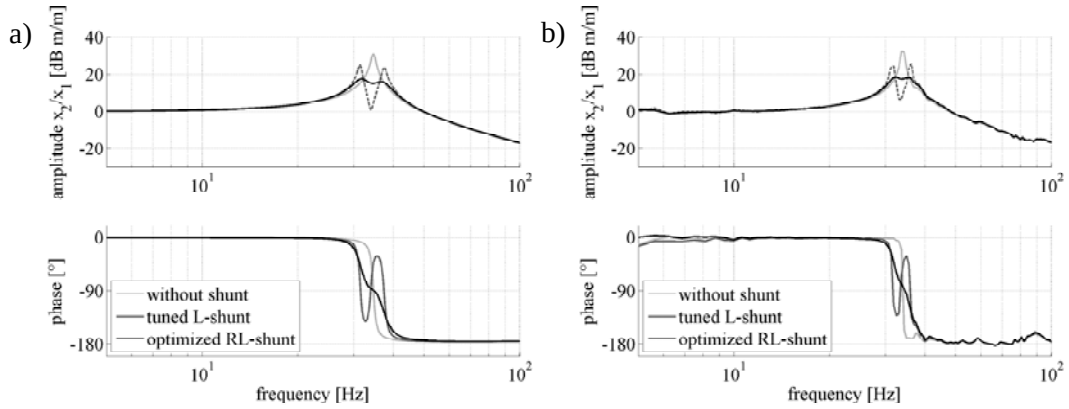

Figure 18. Transmissibility curves of the shunted isolator in a test setup
a) Simulation
b) Measurement

5. CONCLUSIONS

This paper shows the concept, the modeling and the design of a shunted piezoelectric isolator. Thereby, the usefulness of the system in order to positively influence the transmission behavior of an idealized isolation system is shown by simulation and measurement. By using the presented design methodology and simulation model, the required dimensions of the isolator can be affectively estimated. In comparison to measurement results, the quality of the simulation model is proven. First simulation results of a holistic model, in which an elastic description of a base structure is included, show a promising vibration reduction of an excited plane fuselage demonstrator. In a next step, further measurements will be carried out and the presented simulation results will be compared to experimental results on the plane fuselage demonstrator.

6. ACKNOWLEDGEMENTS

The research presented in this paper was performed in the framework of the projects FuMaxSIs (Federal Ministry of Education and Research, Germany), LOEWE AdRIA (State of Hesse, Germany), the PROBRAL program of the DAAD (Germany). The financial support by these projects is gratefully acknowledged. The Brazilian authors acknowledge the CAPES/ Probral, CNPq and INCT for the financial support received during this work.

7. REFERENCES

Antoniou, A., 1969. “Realization of gyrators using operational amplifiers and their use in RC-active-network synthesis”. In *Proc. IEEE 116 1838–50*

Bartel, T., Atzrodt, H., Herold S. and Melz, T., 2010. “Modeling of an Active Mounted Plate by means of the Superposition of a Rigid Body and an Elastic Model”. In *Proceedings of the International Conference on Noise and Vibration Engineering - ISMA*, Leuven, Belgium.

Bartel, T., Baghaie Yazdi, M., Melz, T. and Tarle P., 2011. "Optimization and measurement of a flexible sensitive sensor design". In *Proceedings of the Conference on Smart Structures and Materials - SMART*, Saarbrücken, Germany

Bartel, T., Koch, M., Matthias, M. and Tarle P., 2012. "Simulation, development, and testing of a triaxial vibration isolation platform". In *Proceedings of the International Conference on Noise and Vibration Engineering - ISMA*, pp. 151-162, Leuven, Belgium.

Bastaits, R., Mokrani, B., Preumont, A., 2010. "Control-Structure Interaction in Active Optics of Future Large Segmented Mirrors". In *Proceedings of the International Conference on Noise and Vibration Engineering - ISMA*, Leuven, Belgium.

Behrens, S., Flemin, A. J., Moheimani, S. O. R., 2003."A broadband controller for shunt piezoelectric damping of structural vibration". *Smart Materials and Structures*,12, pages 18-28

Corr, L. R., Clark, W.W., 2001, "Energy Dissipation Analysis of Piezoceramic Semi-Active Vibration Control", In *Journal of Intelligent Material Systems and Structures*, 12, Nr. 11, pages 729-736

De Marneffe, B., Horodinca, M. and Preumont A., 2008. "Vibration isolation via shunted electromagnetic transducers". In *Proceedings of the International Conference on Noise and Vibration Engineering - ISMA*, Leuven, Belgium.

Forward, R. L., 1979, "Electromechanical transducer-coupled mechanical structure with negative capacitance compensation circuit". *US Patent Specification*, 4,158,787

Fuller, C. R., Elliott, S. J. and Nelson ,P.A.,1997. *Active Control of Vibration.* Academic Press.

Hagedorn, P. and DasGupta, A., 2007. *Vibration and Waves in Continuous Mechanical Systems*. John Wiley & Sons Ltd, West Sussex, England.

Hagood, N. W., von Flotov, A., 1991, "Damping of Structural Vibrations with Piezoelectric Materials and Passive Electrical Networks". *Journal of Sound and Vibration*, 146(2), pages 243-268

Herold, S., Atzrodt, H., Mayer, D. and Thomaier, M., 2006. "Modeling Approaches for Active Systems". In *Proceedings of the SPIE, Symposium Smart Structures and Materials and NDE for Health Monitoring and Diagnostics*, No. 6173-24, San Diego, USA.

Hidalgo, I. L., Nabarrete, A. and Santos M., 2011. "Structure-borne transmissibility evaluation through modeling and analysis of aircraft vibration dampers". *Journal of Aerospace Technology and Management*, Vol. 3, No. 2, pp. 147-158.

Konstanzer, P., Grünwalder, M., Jänker, P. and Storm, S., 2006. "Aircraft interior noise reduction through a piezo tunable vibration absorber system". In *Proceedings of the 25th International Congress of the Aeronautical Sciences*, Hamburg, Germany

Lo, W., Hinote, G. and Shih, C., 2002. "Identification of structural operating modes for aircraft cabin noise reduction". In *Proceedings of IMAC-XX: A Conference on Structural Dynamics*, Los Angeles, USA.

Mayer, D., Linz, Ch., Krajenski, V., 2001. "Synthetische Induktivitäten für die semi-passive Dämpfung". *5. Magdeburger Maschinenbau-Tage – Entwicklungsmethoden und Entwicklungsprozesse im Maschinenbau*, Magdeburg

Niederberger, D., 2005. "Smart Damping Materials using Shunt Control". Dissertation, ETH Zürich

Preumont A., 2011. *Vibration Control of Active Structures: An Introduction*. Springer, 3rd edition.

Schmidt, M., Atzrodt, H., Sabirin, C. R., Rue, de, G.J. and Melz, T., 2011. "Comparative operational modal analysis: Application of a semi-active vibration absorber to a manufacturing machine". In: *Proceedings of the 4th International Operational Modal Analysis Conference (IOMAC*), Istanbul, Turkey

Viana, F., Valder, S., 2006. "Multimodal Vibration Damping Through Piezoelectric Patches and Optimal Resonant Shunt Circuits". In *J. of the Braz. Soc. of Mech. Sci. & Eng.* 3, pages 293–310

Wu, S. Y., Bicos A. S., 1997." Structural vibration damping experiments using improved piezoelectric shunts". In Proceedings *of the SPIE, Smart Structures and Materials: Passive Damping and Isolation*, SPIE Vol.3045, pages 40–50, San Diego, USA.

8. RESPONSIBILITY NOTICE

The authors are the only responsible for the printed material included in this paper.